Global NEST Journal, Vol 26, No 6, 05891

Green, environmentally friendly synthesis of MnO nanoparticles for corrosion inhibition in mild steel

Rajasekar V.[1]*, Shyamala M.[2] and Aravind J.[3]
[1]Department of Industrial Biotechnology, Government College of Technology, Coimbatore–641013, Tamil Nadu, India
[2]Department of Chemistry, Government College of Technology, Coimbatore–641013, Tamil Nadu, India
[3]Department of Biotechnology, Saveetha School of Engineering, Saveetha Institute of Medical and Technical Sciences, Saveetha University, Chennai, Tamil Nadu, India
Received: 09/03/2024, Accepted: 15/06/2024, Available online: 20/06/2024
*to whom all correspondence should be addressed: e-mail: rajasekaribtgct@gmail.com
https://doi.org/10.30955/gnj.005891

Graphical abstract

Abstract

This study uses green, environmentally friendly methods to synthesize manganese oxide nanoparticles (MnO-NPs) that can be applied on mild steel as a safe and eco-friendly material with corrosion inhibition attributes. *Mukia madaraspatana* leaf extract is effective in the green synthesis of Mno-NPs. Several critical parameters can influence the corrosion rate and inhibition efficiency of the MnO-NPs, including the dose of nanoparticles in parts per million (PPM), acid concentration, temperature, and exposure time. Response Surface Methodology-Box Behnken Design (RSM-BBD) was employed to optimize these parameters. An optimal dosage of 550 parts per million (ppm) of nanoparticles, an acid concentration of 0.9 M, a temperature of 37°C, and an exposure time of 3.2 hours resulted in an inhibition efficiency of 92.5%. It reduced the corrosion rate to 0.652 (mm/Y) in an independent validation run. These findings demonstrate that the environmentally friendly synthesized MnO-NPs have great potential as an anti-corrosive agent for mild steel.

Keywords: Green synthesis; manganese oxide nanoparticles; environmentally friendly process; response surface methodology; corrosion inhibition

1. Introduction

Plant extract-mediated corrosion inhibitions have been demonstrated, illustrating plant extract-mediated nanoparticles as corrosion inhibitors have acquired the best-restrained attention. Lately, nanotechnology has grown to be one of the quickest-rising technologies in the world owing to its remarkable improvements in the physical, chemical, mechanical, and optical properties of matter reduced to a nanometer in size. Nanotechnology has performed a critical role in developing novel materials with precise physiochemical properties for feasible solicitation. Nanoparticles (NPs) of the desired shape, size, and functionality can be synthesized using two indispensable techniques: top-down and bottom-up. In the top-down technique, nanomaterials are synthesized through various preparative methods like ball milling, lithographic techniques, and etching. Later, NPs were produced from simpler molecules, including multiple approaches like sol-gel processes, spray pyrolysis, chemical vapor deposition, and laser pyrolysis. However, these techniques are expensive, pose risks to human health and the ecosystem, and are much less proficient. To counter the harm, a new era of green synthesis came to light in recent research and development in material science (Ying *et al*. 2022; Can 2020; Amodu *et al*. 2022).

Plants have been widely considered for the synthesis of metallic nanomaterials due to the prevalence of potential phytochemicals in several plant extracts, for instance, flavones, ketones, carboxylic acids, amides, phenols, aldehydes, ascorbic acids and terpenoids which are efficient to reduce metal salts into metallic NPs. Also, these materials encompass electron-rich atoms akin to those endowed in chemical corrosion inhibitors, which contribute a significant surface area for synergy on the steel. Nano-manganese oxides are one of the assuring nanomaterials due to their high surface area and adsorption capacity, low toxicity, cost, durability, and flexibility. They are applied for board spectrum as catalysts and environmental treatment, and they find their niche in

corrosion protection (Basik*et al*. 2020; Dash*et al*. 2023; González*et al*. 2021).

Mukia maderaspatana is a member of the family Cucurbitaceae of the genus Mukia, which is in the kingdom Plantae of the division Dermatophytes, sub-division Angiospermae of the class Dicotyledonae, subclass polypetalae of series Calyiflorae, and subclass sympetalae of class Dicotyledonae. In Sri Lanka and India, this plant expands extensively. It is known locally as mosumosukai or musumusukkai in Tamil Nadu, and its English name is Madras pea pumpkin or rough bryony. Its symmetrical oval leaves are 3 to 5-lobed and are 3 to 9 cm long. The leaves of *M. maderapatana* include additional substances such as carbohydrates, steroids, tannins, and flavonoids in addition to 4-methylpentyl ester, 4-methoxybutyn-1-ol, and dichloroacetic acid. Mukia leaves, fruits, and flowers are used as medicine in Siddha and Ayurveda to treat ulcers, inflammation, hyperglycemia, cough, hepatic disorder, etc. Mukia leaves also help cattle digest and act as an immunological booster (Chitra *et al*. 2015; Devi and Sathishkumar 2017).

Mild steel (MS), low carbon steel is appreciably applied in industries since it's distinctly less expensive to produce and has good weldability, machinability, ductility, and toughness in the real-time world, including automobile body components, pipelines, buildings, structural shapes, ships, bridges, pots and pans used for cooking, railway lines, and tin cans, etc., (Birat 2020; Chandel *et al*. 2023; Kim *et al*. 2022). MS is widely applied in real-time, but its serviceability depends on the initial corrosion attack. Corrosion of MS is a spontaneous process arising out of chemical or electrochemical interactions with the encircling environment. Hydrochloric acid solutions are employed in industries for applications including acid pickling, cleaning of boilers, oil and well acidizing, ore production, petrochemical processes, and acid descaling, which consequently affects the device and equipment by corrosion due to its high concentration (Raabe 2023; Eliaz 2019). Corrosion substantially results in material loss, which is critical in determining engineered products' performance, life cycle, safety, and cost. One of the most traditional methods to hinder metallic corrosion is corrosion inhibitors. Synthetic inhibitors are highly effective since they contain multiple bonds and heteroatoms, but their applicability raises questions concerning safety, toxicity, public health, and eco-friendly nature. As they aren't economically feasible, researchers focused on using green environmental benign corrosion inhibitors that are biodegradable, non-toxic, readily available, and inexpensive. Active constituents such as tannins, polysaccharides, proteins, amino acids, and pigments are present in natural green inhibitors that protect metals by adhering them to their surface. Plant extracts that inhibit corrosion have been illustrated for efficacy (Kartsonakis and Charitidis 2020; Akinbulumo *et al*. 2020; Al-Amiery *et al*. 2022; Heidarzadeh *et al*. 2021).

One of the most significant statistical methods for evaluating trials that evolve in many ways and are impacted by various distinct variables is the response surface method (RSM), which establishes the optimal process parameters. Most studies have solely examined how inhibitors can reduce corrosion using conventional approaches. The literature addresses a small and insufficient optimization of corrosion inhibitors using RSM. Thus, it is still necessary to determine the circumstances in which an inhibitor will function at its finest and yield the most significant reaction. RSM's main benefit is that it minimizes the number of experimental runs needed to identify the ideal condition (Aravind *et al*. 2016; Mohamed *et al*. 2023; Kamaraj *et al*. 2024).

In this research work, an attempt was made to formulate an environmentally friendly process of creating nanomaterial for corrosion inhibition. Nano-manganese oxides were synthesized using potassium permanganate with *Mukia madaraspatana* leaf extract, and the manganese oxide NPs were characterizedby UV-visible spectral analysis, X-ray diffraction analysis (XRD), and Fourier-transform infrared (FTIR) analysis. The potency of manganese oxide nanoparticle as a corrosion inhibitor in MS, when exposed to acid, was measured by the RSM method to optimize the four parameters selected using central composite design (BBD), namely the temperature, acid concentration, inhibitor concentration, and immersion time with weight loss and inhibition efficiency as outputs.

2. Materials and methods

2.1. Preparation of mukia madaraspatana leaves extract

The *Mukia madaraspatana* leaves were collected along the riverside from Coimbatore, Tamil Nadu, India. The collected leaves were washed with distilled water to get rid of impurities like dust and scum from the surface of the leaves and were dried and ground to get fine *Mukia madaraspatana* leaf powder. Initially, 25 g of fine *Mukia madaraspatana* leaves powder was dispensed in 100 mL of deionized water andsoaked overnight. Then, the resultant solution was further refined with Whatman (N1) filter paper, and the *Mukia madaraspatana* leaves extract solution was saved for further use (Chitra *et al*. 2015; Devi and Sathishkumar 2017; Kalaiyarasi *et al*. 2024).

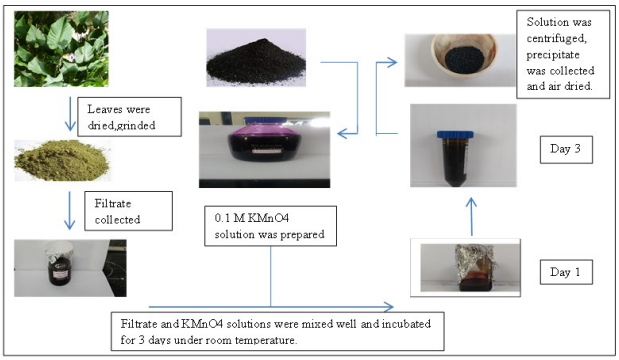

Figure 1. Systematic representation of manganese oxide nanoparticles (MnO-NP) synthesis

2.2. Green synthesis of MnO NPs

The extract from *Mukia madaraspatana* leaves of 15 mL was mixed with precursor 0.1 M $KMnO_4$ (85 mL). The above solution was stirred for about 45 minutes using a magnetic stirrer at 1600 rpm. Afterward, the prepared solution was

incubated at room temperature for 3 days, changing its color to reddish brown, confirming the formation of MnO NPs; these were further centrifuged at 2500 rpm for 10 minutes, and the resulting pellet was accumulated, washed, and dried in a hot air oven for about 5 h at 150°C and then calcinated at 500°C for 3 h in a muffle furnace. The succeeding fine powder became MnO-NPs (Chitra *et al*. 2015; Kalaiyarasi *et al*. 2024). Figure 1 portrays the synthesis flow of MnO-NP.

2.3. Characterization techniques

UV-visible analysis was performed in a spectrophotometer on a 200-650 nm wavelength range to investigate the optical absorbance and emission spectra of prepared MnO NPs. The phase and crystal structure of the synthesized MnO NPs were determined by utilizing X-ray diffraction X-Pert Pro PANalytical using Cu as a radiation source. Fourier Transform infrared spectroscopy (FTIR) SHIMADZU (Miracle 10) was employed to examine the functional group of the dried NPs over a wave number range of 400-4000 cm^{-1}. A field emission scanning electron microscope (FESEM) inspected particle size and morphology (Amodu*et al*. 2022; Tamilselvi *et al*. 2023).

2.4. Preparation of steel specimen and corrosion solution

The MS coupons of dimension 1 × 5 × 0.2 cm were used for corrosion studies due to their exemplary applications in industrial sectors. The surface of the steel coupons was polished by utilizing a bench grinder to remove the existing passive film. The polished coupons were stored in sealed bags inside moisture-free desiccant (silica) until needed.1 M HCl solution was prepared by diluting analytical grade 37% HCl with deionized water. Then, 1000 mg of the MnO-NP powder was dispensed in 1000 mL of 1 M HCl (stock solution). All corrosion experiments, including and excluding the inhibitor at varied concentrations ranging from 200 to 600 ppm, were executed using this 1 M HCl solution (Amodu*et al*. 2022; Tamilselvi *et al*. 2023; Fadl *et al*. 2020).

2.5. Corrosion tests by weight loss method

MS coupons1 × 5 × 0.2 cm were weighed, immersed by suspension method in 100 mL of test solution made up of 1 M HCl without (blank) and with inhibitor (MnOnps), and sealed to eliminate air. The containers were placed in a water bath equilibrated to 308 K for 3 h, after which they were withdrawn and cleaned and then re-weighed to determine the weight loss. Triplicates of experiments were carried over to estimate the mean weight loss (Δw) employed to evaluate corrosion rate (CR) and Corrosion inhibition efficiency (I_W) using equations (3) and (4)

$$CR = \frac{87600\,\Delta w}{\rho A t} \tag{3}$$

$$I_w = \frac{100\left(1 - CRinh\right)}{CRHCl} \tag{4}$$

Where A, t, ρ represent surface area (cm^2), immersion time in hours (h), and density (gcm^{-3}), respectively, $CR_{inh}$and CR_{HCl} refer to corrosion rate in the 1 M HCl with inhibitor and without inhibitor. Similar procedures were repeated at different temperatures, acid concentration, time, and inhibitor concentration were recorded (Al-Amiery *et al*. 2022; Boudalia *et al*. 2023).

2.6. Surface and corrosion product analysis

After 12 hours of immersion of MS in the presence and absence of inhibitor in 1 M HCl acid solution, the withdrawn MS surface was cleaned, and the deposits on the MS coupon were carefully scraped off and analyzed by UV and FTIR spectroscopy. FESEM and EDS observed surface morphology, topography, and other features that determined the surface's elemental composition (Tamilselvi *et al*. 2023; Fadl *et al*. 2020).

2.7. Design of experiment and modeling: Response Surface Methodology

The scientific problem-solving approach involves a systematic and thorough approach that uses principles and methodologies called Design of Experiment (DOE); this ensures that the engineering findings drawn are legitimate, defensible, and supported. Furthermore, all these tasks are performed while limiting the usage of engineering runs, time, and financial resources. One such method is Response Surface Methodology (RSM) (Aravind *et al*. 2016; Mohamed *et al*. 2023; Kamaraj *et al*. 2024).

The experiment enables us to approximate interaction and quadratic effects, providing insights into the (local) configuration of the response surface under investigation. Due to this rationale, they are referred to as RSM. Under RSM Box–Behnken designs (BBD) arefavoredfor optimizing process parameters. The Box-Behnken design is a quadratic design capable of rotation and necessitates three layers for each element. Compared to the central composite designs, the designs have a restricted capacity for orthogonal blocking (Sandhu *et al*. 2022; Mohamed *et al*. 2023).

Design Expert software was used to design the model, procure statistical output, and obtain quadratic polynomial equations.

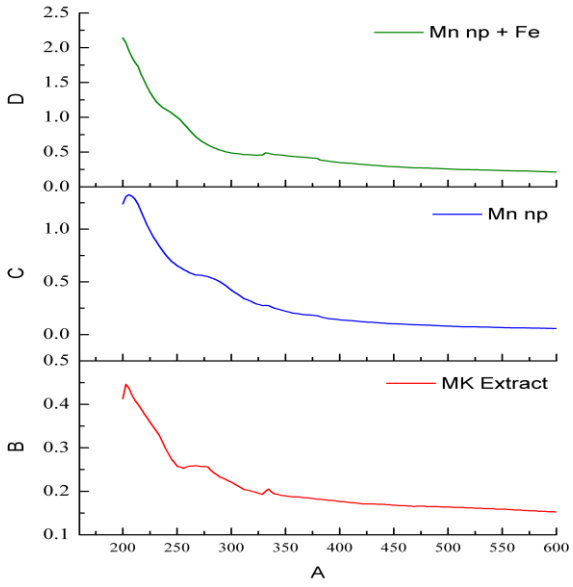

Figure 1. UV-visible spectra of MnOnps

3. Results and discussion

3.1. Characterization of MnO NPs

UV-visible spectroscopy is an analytical tool used to characterize nanoparticles based on electron transition from lower to higher energy levels after ultraviolet and visible radiations are absorbed (Gunavathyand Murugavel 2012). From Figure 1, the maximum absorption was noted for the wavelength 328 nm (λ_{max}), confirming the formation of MnOnps.The formation of a complex between Cys/Ag-Au NCz and Fe was verified using UV-visible spectroscopy by Basik *et al*. (2020); two distinct peaks in its spectrum at wavelengths of 208.7 nm and 248.2 nm were noted before immersing the mild steel coupon. However, after immersing the mild steel coupon, the solution showed a noticeable shift in wavelength to 225.5 nm and 253.0 nm. The rise in the peaks' absorbance indicates a strong development of complexes between the metal and inhibitor in an acidic environment. In the current work, there was a notable shift in the spectrum and the intensity due to the interaction of nanoparticles with MS.

In the FTIR spectra (Figure 2), the bands at 686 and 948 cm^{-1} were linked with the C=C functional group, bands at 1149 and 1381 cm^{-1} were recognized to C-O and O-H stretching, O-H stretching was apportioned to physisorbed H_2O molecules on the MnO surface. The occurrence of these functional groups donates to corrosion prevention in MS. Two peaks with low intensity at 416 and 455 cm^{-1} suggest the existence of MnO stretching mode. The decrease in the intensity of a peak in FT-IR spectra is due to the mineral structure of Mn-O, which has stronger bonds and weak vibrations. Basik *et al*. (2020) prepared silver-gold nanoparticles and analyzed them using FTIR in their study on corrosion prevention. They observed a peak at 3427cm^{-1} for N-H stretching vibration of the NH^{3+} group in the cysteine functionalized Ag-Au nanocomposite. The peak observed at 2341 cm^{-1} corresponds to the vibration of the S–H bond in the thiol group.In addition, the peaks detected at 1740 cm^{-1}, 1639 cm^{-1}, and 1460 cm^{-1}indicate the presence of the functional groups amide I, II, and III, respectively. A signal observed at 1020 cm^{-1} signifies the vibration of the cysteine S-O bond. Cysteine molecules S-, COO-, and NH^{3+} resulted in a bonding contact between the Au-Ag, as evidenced by the lower frequencies at 663 cm^{-1} and 520 cm^{-1}.

Kartsonakis and Charitidis (2020) utilized hybrid materials in their study on corrosion prevention in mild steel. The FTIR analysis revealed the presence of metal-oxygen bonds throughout the frequency range of 400 to 1000 cm^{-1}. The TiO_2 displayed absorption peaks at 496, 567, 674, and 760 cm^{-1}. The typical peaks of CeO_2 were seen within the spectral region of 425 to 540 cm^{-1}. The wide spectral bands ranging from 3100 to 3324 cm^{-1} are caused by the stretching vibration of the O–H bond of the physically adsorbed water found in the sample. The peaks detected at 1557 and 2910 cm^{-1} are ascribed to the N-H deformation/bending and stretching vibrations, respectively. The C=N stretching vibration was seen at the wavenumbers 1460, 1605, and 2100 cm^{-1}. The presence of C-N was confirmed by the peaks found at 1060 and 1306 cm^{-1}. The peaks observed at 787 and 1005 cm^{-1} indicate the C-S stretching vibrations. The presence of C=S stretching vibrations may be observed through the peaks at 1145 and 1236 cm^{-1}.

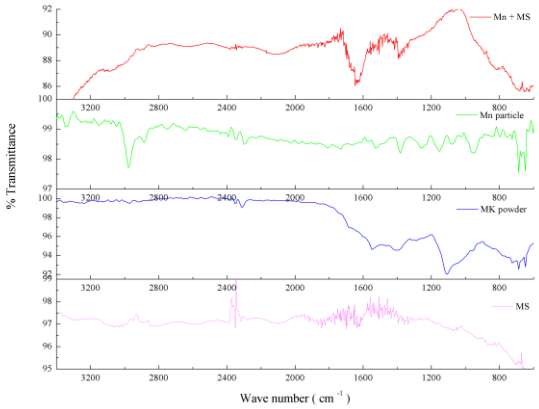

Figure 2. FTIR spectra of MnOnps

Figure 3 represents the x-ray diffraction (XRD) pattern of MnOnps measured over 10-80°. The pattern reveals the plane of reflection at 110, 211, 541. Strong diffraction is evident in the crystalline structure of synthesized MnOnps of 16 nm. In the XRD pattern, no other diffraction peaks were observed, which further ascertained the high purity of the samples.

Fada *et al*. (2020), in their preparation of corrosion preventive hybrid nanocomposite material and their XRD analysis, exposed the occurrence of distinct peaks at definite angles (2θ), indicating the presence of the Anatase phase structure.

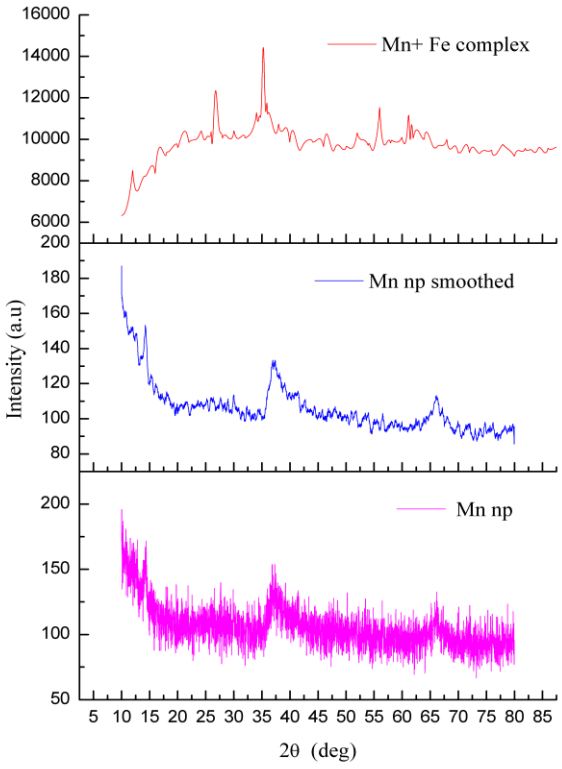

Figure 3. XRD pattern of MnOnps

The ICDD-PDF database was utilized to identify the crystalline phases that developed on the surface of acid treated Mild steel. The mild steel surface's corrosion product in an HCl acid solution is displayed. The existence of iron oxide is suggested by the peak at 2θ (35.5°, 59.9°, 71.7°), which caused corrosion. Mild steel diffraction pattern after being submerged in a test solution containing 550ppm manganese nanoparticles. Iron oxides are not present, as seen by the iron peaks at 2θ (44°, 65°). These observations clearly show that when MnO is present, adsorbed protective film forms on the metal surface. DOI:10.1016/j.arabjc.2013.08.011

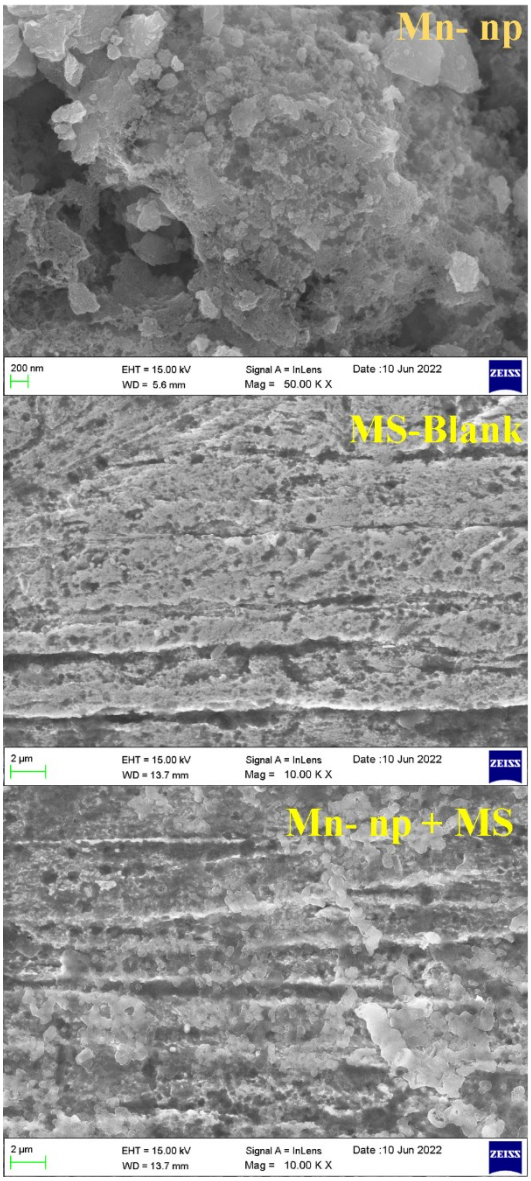

Figure 4. SEM analysis of Sample MS, Nanoparticle, and nanoparticle-bound MS

3.2. Surface analysis and mechanistic studies

The surface shape and size of MnO nanoparticles are determined using SEM examination, as shown in Figure 4. The average particle size determined through SEM analysis was 40 nm and had a spherical shape. The size of MnO nanoparticles is increased due to the aggregation and accumulation resulting from their more extensive surface area and higher quantity. The previous work found that manganese oxide nanoparticles, produced using pineapple peel extract, exhibited a spherical shape with a size range of 40-50 nm (Klinbumrung *et al*. 2022). This finding aligns well with the results of the current investigation.

SEM analysis was performed for MS steel surfaces withdrawn from both inhibited and uninhibited 1 M HCl, and their morphologies are depicted in Figure 4. The corrosion attack was so harsh that cracks and pits appeared on the surface of MS with scratches when the inhibitor was not added. Still, when the inhibitor was added, the surface was reasonably smooth, free of pits and cracks, with only slight corrosive damage. Hence, it is evident that MnO NPs have great potential to inhibit the corrosion of MS, though they don't wholly eradicate corrosion. The elemental composition of the MS surface after 12 h of immersion time in 1 M HCl containing the MnO NPs was depicted and compared with the surface retrieved from the uninhibited acid solution. The SEM pictures published by Basik *et al*. [13] show the presence of silver-gold in a spherical amorphous shape, accompanied by irregularly shaped particles of functionalized cysteine in the surrounding area. The FE-SEM images from Yang *et al*. [27] demonstrated that the presence of dislocations at the interface between nanoparticles and the polymer network led to the formation of micro-holes. These micro-holes, in turn, facilitated the development of passivation micro-cracks, effectively preventing the progression of destructive macro cracking in the coatings. The SEM photos of Mild Steel with hybrid material, as assessed by Kartsonakis and Charitidis (2020), revealed the formation of spongy agglomerations in many layers on the surface. Multiple lamellar structures are found, attributed to the hematite and goethite α phases. The presence of a ruptured layer suggests that the inhibitor has interacted with the metal surface.

3.3. Mechanism

MnO-NPs and *Mukia madaraspatana* leaf extract dissolved in HCl are transported toward the surface of MS, where hydrogen ions and ferrous ions are produced by reduction on the cathodic and anodic active sites, respectively.

$$2H^{+} + 2e^{-} \rightarrow H_2$$

$$Fe \rightarrow Fe^{2+} + 2e^{-}$$

Also, when exposed to the atmosphere, the dissolved oxygen in the HCl solution gets reduced to water molecules by a cathodic reaction.

$$O_2 + 4H^{+} + 4e^{-} \rightarrow 2H_2O$$

The presence of a functional group in *Mukia madaraspatana* leaf extract, consisting of carbon, oxygen, and nitrogen atoms, facilitates the interaction between MnO nanoparticles and Fe^{2+} ions. This interaction leads to the formation of a complex at the interface of the MS/HCl solution, specifically the Fe^{2+}+ MnO^{-}*Mukia madaraspatana* leaf extract complex. This complex occupies the anodic active sites and prevents the formation of ferrous ions, thereby inhibiting corrosion. The adsorption mechanism of

Mn-O nanoparticles on the MS surface is primarily due to physisorption, which involves an electrical contact between the electrons deposited on the MS on its surface; this promotes the movement of electrons from the d orbitals of Fe (iron) to the non-bonding π orbitals in the inhibitor molecules. As a result, the adsorption of inhibitor molecules onto the mild steel surface is increased, as stated in their work (Lai *et al*. 2017; Edoziuno *et al*. 2020). Gunavathy and Murugavel (2012) explored the competence of Musa Acuminata fruit peel extract as a corrosion inhibitor for mild steel in 1N HCL. There was a 92% inhibition on corrosion at 30°C, but there was weight loss due to corrosion when the temperature was increased, and the inhibitory effect of the extract decreased by up to 2%. In their study, Lai *et al*. (2017) investigated the use of synthetic inhibitor combinations to stop the corrosion of mild steel in HCl. They found that the effectiveness of the inhibitors declined as the temperature and acid concentration increased. Akinbulumo *et al*. (2020) noted that while using an extract from Euphorbia heterophylla as a corrosion inhibitor for mild steel in 1.5 M HCl, the effectiveness of inhibition first rose with increasing temperature over the examined immersion duration but eventually decreased. Farhadian *et al*. (2020) have documented a corrosion inhibitor for mild steel derived from castor oil for use in an acidic environment. This inhibitor has successfully addressed the limited effectiveness exhibited by several inhibitors at high-temperature conditions. The approach achieved the highest efficiency of 62.56% in this investigation.

3.4. RSM modelling and optimization

Factors that could impact and influence the corrosion rates and inhibition efficiency in MS were explored for their impact under varying ranges of each parameter when green synthesis MnO-NPs were investigated for their potency to impede corrosion and enhance the efficiency of inhibition of corrosion by these MnO-NPs. Table 1 represents the design, the factors taken for the study (MnO-NP dosage, acid concentration, temperature, and time), and the response: corrosion rate (R1) and inhibition efficiency (R2).

Table 1. Design of RSM BBD

	Factor 1 A:Nanoparticle dosage (PPM)	**Factor 2 B:Acid concentration**	**Factor 3 C: Temperature**	**Factor 4 D:Time (h)**	**Response 1 Corrosion rate (mm/Y)**	**Response 2 Inhibition efficiency**
Run		(M)	(°C)			(%)
1	400	1	50	4.5	81.66	71.82
2	600	0.5	50	4.5	40.45	91.66
3	200	1.5	50	4.5	14.1	78.79
4	200	1	65	4.5	1.2	44.18
5	400	1.5	65	4.5	95.81	67.7
6	400	1	35	3	106.54	64.13
7	400	0.5	35	4.5	72.23	81.58
8	600	1	50	6	203.42	28.01
9	600	1.5	50	4.5	201.65	32.7
10	400	1.5	50	3	45.57	61.12
11	400	1	50	4.5	80.86	68.14
12	400	0.5	50	6	24.21	40.38
13	600	1	35	4.5	102.08	63.46
14	400	1.5	35	4.5	118.28	72
15	400	1.5	50	6	167.05	72.12
16	600	1	65	4.5	139.07	39.52
17	200	1	50	6	0.81	34.6
18	400	1	65	6	108.69	50.92
19	200	0.5	50	4.5	72.77	22.31
20	400	0.5	65	4.5	42.18	62.4
21	400	1	65	3	29.62	52.14
22	200	1	35	4.5	86.05	52.78
23	200	1	50	3	97.47	42.75
24	400	1	50	4.5	82.59	71.11
25	400	1	50	4.5	82.59	69.2
26	400	0.5	50	3	89.65	75.32
27	400	1	50	4.5	83.96	70.71
28	600	1	50	3	39.81	56.16
29	400	1	35	6	84.8	53.22

Table 2 depicts the ANOVA output for evaluating variables explored on the response 1 (R1) corrosion rate. P-values less than 0.05 indicate model terms are significant. Nanoparticle dosage (A), acid concentration (B), temperature (C), time (of exposure) (D), interaction between MnO-NP dosage with acid concentration (AB),

MnO-NP dosage with temperature (AC), MnO-NP dosage with time of exposure (AD), acid concentration with time (BD), and Temperaure with time (CD) are significant model terms; they impact the outcome of the experiment: influence the nanoparticle impact on decreasing corrosion rate and increase inhibition of correction.

Table 2. ANOVA output for Response 1: Corrosion rate

Source	Sum of Squares	df	Mean Square	F-value	p-value	
Model	73423.66	10	7342.37	1585.36	< 0.0001	significant
A-Nanoparticle	17182.39	1	17182.39	3710.02	< 0.0001	
B-Acid concentration	7548.58	1	7548.58	1629.89	< 0.0001	
C-Temperature	1961.22	1	1961.22	423.47	< 0.0001	
D-Time	2709.61	1	2709.61	585.06	< 0.0001	
AB	12085.70	1	12085.70	2609.54	< 0.0001	
AC	3711.25	1	3711.25	801.33	< 0.0001	
AD	16935.12	1	16935.12	3656.63	< 0.0001	
BC	14.36	1	14.36	3.10	0.0952	
BD	8734.77	1	8734.77	1886.01	< 0.0001	
CD	2540.66	1	2540.66	548.58	< 0.0001	
Residual	83.36	18	4.63			
Lack of Fit	79.18	14	5.66	5.40	0.0577	not significant
Pure Error	4.19	4	1.05			
Cor Total	73507.03	28				

Table 3. ANOVA for Quadratic model Response 2: Inhibition efficiency

Source	Sum of Squares	df	Mean Square	F-value	p-value	
Model	8451.42	14	603.67	32.77	< 0.0001	significant
A-Nanoparticle	108.60	1	108.60	5.90	0.0292	
B-Acid concentration	9.68	1	9.68	0.5258	0.4803	
C-Temperature	411.96	1	411.96	22.37	0.0003	
D-Time	436.45	1	436.45	23.70	0.0002	
AB	3331.60	1	3331.60	180.88	< 0.0001	
AC	58.83	1	58.83	3.19	0.0956	
AD	100.00	1	100.00	5.43	0.0353	
BC	55.35	1	55.35	3.01	0.1050	
BD	527.62	1	527.62	28.65	0.0001	
CD	23.47	1	23.47	1.27	0.2779	
A^2	2332.82	1	2332.82	126.65	< 0.0001	
B^2	38.33	1	38.33	2.08	0.1712	
C^2	121.36	1	121.36	6.59	0.0224	
D^2	1177.00	1	1177.00	63.90	< 0.0001	
Residual	257.87	14	18.42			
Lack of Fit	236.32	10	23.63	4.39	0.0835	not significant
Pure Error	21.55	4	5.39			
Cor Total	8709.29	28				

P-values *less than 0.0500 indicate model terms are significant. Nanoparticle dosage (A), temperature (C), time (of exposure) (D), the interaction between MnO-NP dosage with acid concentration (AB), Nanoparticle dosage with time (AD), acid concentration with time (BD), Dosage^2 (A^2), temperature^2 (C^2), time^2 (of exposure) (D^2) were significant model terms, which impacted the inhibition efficiency.*

Figure 5 portrays the normal plot of expected vs. actual values obtained after running the RSM BBD; a robust and positive correlation existed between the expected and actual values.

$$\begin{aligned} \textit{Corrosion rate} = {} & 82.51 + 37.84 * A + 25.0808 * B \\ & + -12.7842 * C + 15.0267 * D + 54.9675 * AB + 30.46 * AC \\ & + 65.0675 * AD + 1.895 * BC + 46.73 * BD + 25.2025 * CD \end{aligned} \quad (5)$$

The polynomial quadratic equation Eq.5 depicts the correlation and the impact of each variable involved in the design on the outcome and the effect of nanoparticles on the corrosion rate; this matches the ANOVA output in Table 2. Figure 6 portrays the 3D contour plots of iteration of each variable of the impact on corrosion rate; Figure 6a [dosage (A) vs. acid concentration (B)], Figure. 6b [acid concentration (A) vs. temperature (C)], Figure 6c [dosage (A) vs. time (D)], Figure 6d [acid concentration (B) vs. temperature (C)], Figure 6e [acid concentration (B) vs time (D)] and Figure 6f [temperature (C) vs time (D)]. The quadratic equation fit for the model predicted an R^2 Value of 0.9956 for response 1, and the quadratic fit for Inhibition efficiency predicted an R^2 value of 0.938 for response 2.

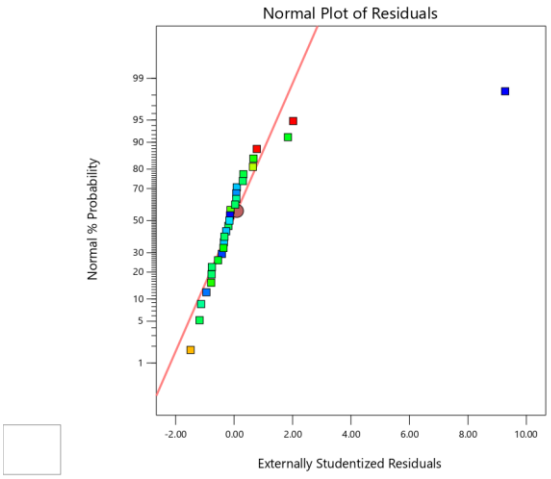

Figure 5. Normal plot of corrosion rate (expected vs. actual)

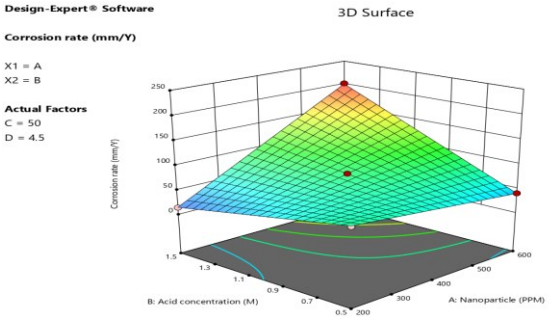

Figure 6a. 3D contour plot depicting the impact of acid concentration and nanoparticle dosage on corrosion rate

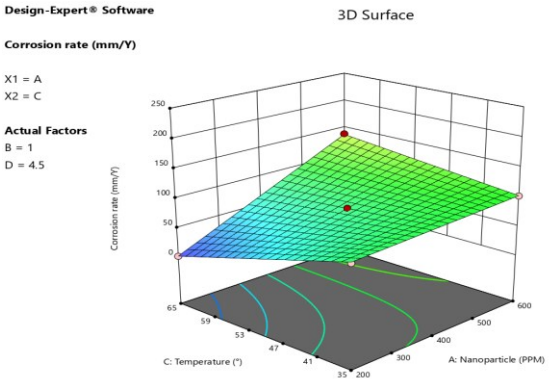

Figure 6b. 3D contour plot depicting the impact of temperature and nanoparticle dosage on corrosion rate

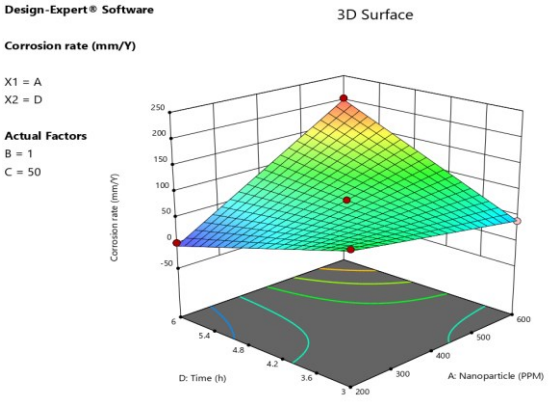

Figure 6c. 3D contour plot depicting the impact time and nanoparticle dosage on corrosion rate

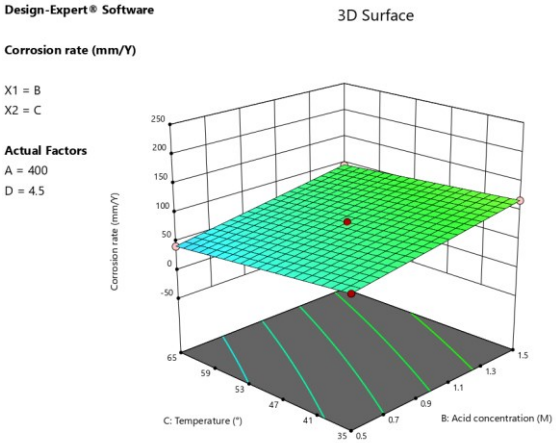

Figure 6d. 3D contour plot depicting the impact of temperature and acid concentration on corrosion rate

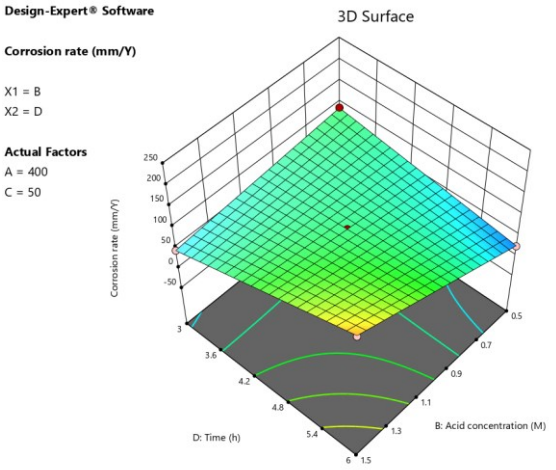

Figure 6e. 3D contour plot depicting the impact of time and acid concentration on corrosion rate

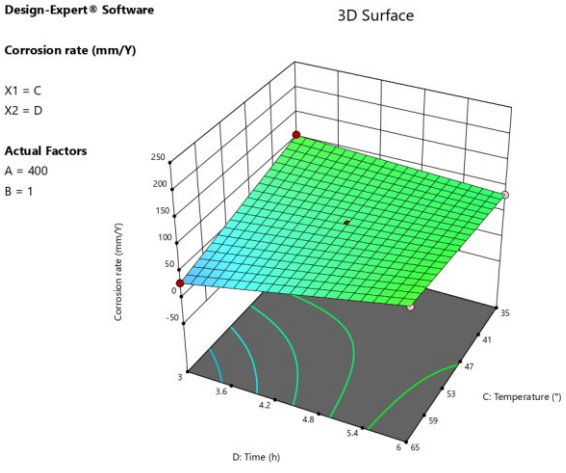

Figure 6f. 3D contour plot depicting the impact of time and temperature on corrosion rate

Edoziuno *et al*. (2020) described refining and developing prediction models to prevent the corrosion of mild steel in sulphuric acid using Methyl-5-benzoyl-2-benzimidazole Carbamate (Mebendazole). Analyzed using Design Expert, the corrosion inhibition process parameters were assessed, encompassing corrosion penetration rate, inhibition efficiency, inhibitor concentration, acid concentration, weight loss, and their interrelationships. The corrosion

inhibition process parameters were optimized, and predictive mathematical models were developed using the Response Surface Methodology (RSM) with the central composite design (CCD). A quadratic model was created, which predicted an ideal inhibitory efficacy of 88.5%. Our investigation found that using a dosage of 500 to 550 ppm of MnO-NP, with an ideal acid concentration of 1M, effectively reduced corrosion to a significant degree; this was achieved by maintaining a controlled temperature of 35 to 37°C for a duration of 3 to 3.2 hours.

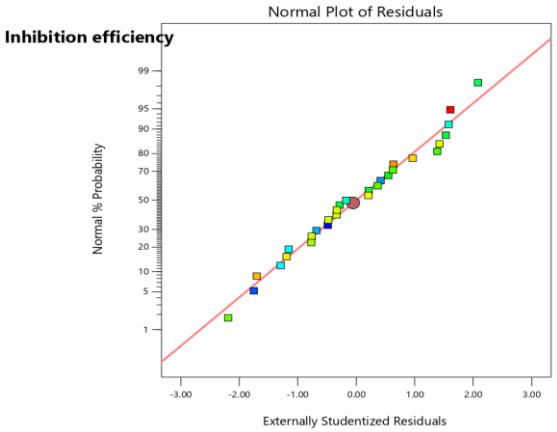

Figure 7. Normal plot of inhibition efficiency (expected vs. actual)

Figure 7 depicts the normal plot of expected vs. actual value obtained after running the RSM BBD, and there was a strong and positive correlation between the predicted and actual values of inhibition efficiency (R2).

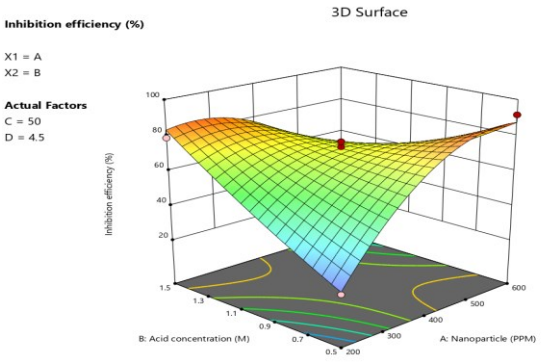

Figure8a. 3D contour plot depicting the impact of acid concentration and nanoparticle dosage on the inhibition efficiency

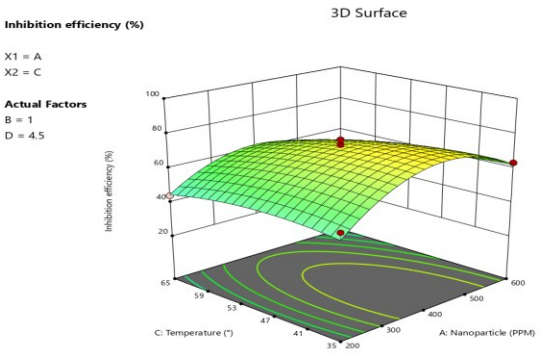

Figure 8b. 3D contour plot depicting the impact of temperature and nanoparticle dosage on the inhibition efficiency

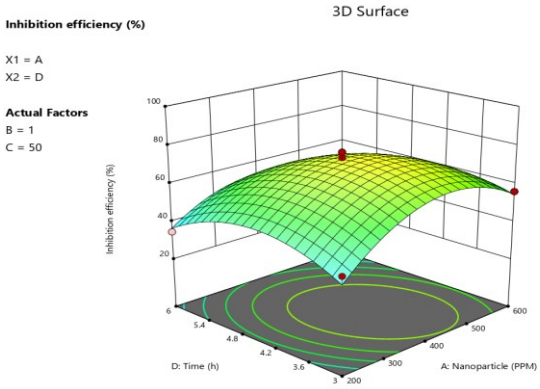

Figure 8c. 3D contour plot depicting the impact of time and nanoparticle dosage on the inhibition efficiency

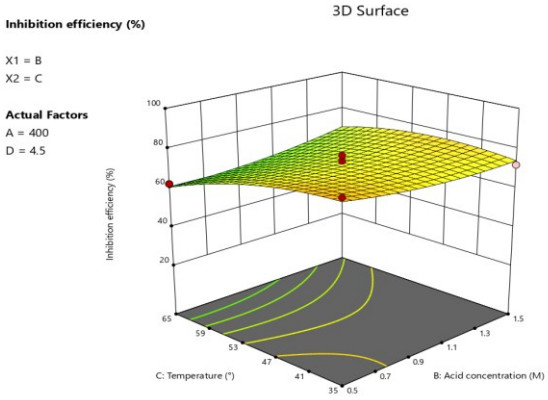

Figure 8d. 3D contour plot depicting the impact of temperature and acid concentration on the inhibition efficiency

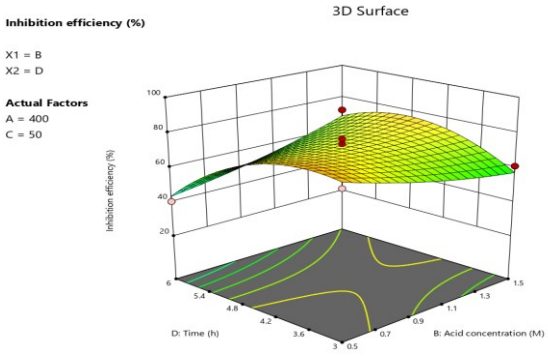

Figure 8e. 3D contour plot depicting the impact of time and acid concentration on the inhibition efficiency

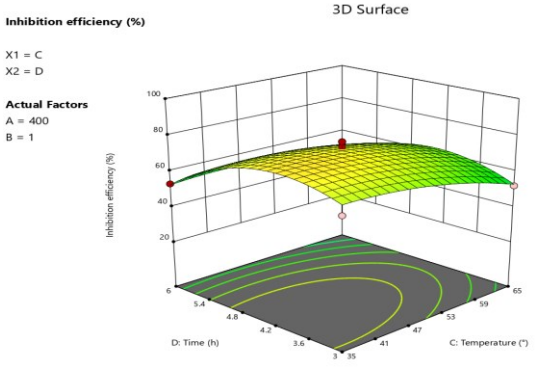

Figure 8f. 3D contour plot, depicting the impact of time and temperature on the inhibition efficiency

$$Inhibitionefficiency = 72.996 + 3.00833 * A + 0.898333 * B + -5.85917 * C + -6.03083 * D + -28.86 * AB + -3.835 * AC + -5 * AD + 3.72 * BC + 11.485 * BD + 2.4225 * CD + -18.9642 * A^2 + 2.43075 * B^2 + -4.3255 * C^2 + -13.4705 * D^2 \quad (6)$$

The polynomial quadratic equation Eq.6 represents the correlation and the impact of each variable involved in the design on the outcome of the effect of nanoparticles on the inhibition efficiency, and this matches the ANOVA output in Table 3. Figure 8 portrays the 3D contour plots of the interaction of each variable of the impact on inhibition efficiency; Figure 8a [dosage (A) vs. acid concentration (B)], Figure 8b [acid concentration (A) vs. temperature (C)], Figure 8c [dosage (A) vs. time (D)], Figure 8d [acid concentration (B) vs. temperature (C)], Figure 8e [acid concentration (B) vs time (D)] and Figure 8f [temperature (C) vs time (D)].

Souri *et al*. (2018) utilized response surface methodology (RSM) to optimize the green production of manganese oxide nanoparticles (MnO NPs) using an extract from *Dittrichia graveolens* (L.). The central composite design was employed to assess the impact of pH, duration, and the ratio of extract to metal on the synthesized nanoparticles (NPs). Based on the p-values (< 0.05), it is evident that the extract-to-metal ratio was the most influential parameter. The researchers have identified the ideal conditions: 56.7 minutes, a pH of 7.2, and an extract-to-metal ratio of 87.9 v/v. Manganese oxide nanoparticles (NPs) were utilized optimally to degrade industrial dyes. These NPs exhibited significant activity in degrading Rhodamine B and light green dye. The average size of the synthesized MnO nanoparticles under optimum conditions was reported to be approximately 38 nm. Amodu *et al*. (2022) employed Banana (Musa paradisiaca) peel extract (BPE) as a corrosion inhibitor for mild steel in a 1.0 M HCl solution to minimize environmental impact. The impact of concentration and temperature on the effectiveness of inhibition was analyzed and improved using response surface methodology (RSM) and artificial neural network (ANN). The numerical optimization of RSM yielded an optimal corrosion inhibition efficiency of 60.08% at a temperature of 308.08 K and a concentration of 7.44 g/L.

In our study, an independent run was made to check the validity of the optimized parameter to obtain the best result of maximum inhibition of 83% and least corrosion rate of 0.6. With an optimal nanoparticle dosage of 550 ppm, acid concentration of 0.9 M, temperature of 37°C and exposure time of 3.2 hours imparted an inhibition efficiency of 92.5% and minimized corrosion rate to 0.652 (mm/Y) was achieved on an independent run (validation run).

4. Conclusion

Mukia madaraspatana leaf extract was successfully demonstrated in this work for an environmentally friendly green synthesis of Manganese oxide nanoparticles (MnO-NPs). FTIR, XRD, and SEM-based characterization of the MNnO-NP was executed, and the suitability of the nanomaterial for application as an anti-corrosive agent was revealed. The optimization experiments by RSM-BBD provided optimal values for all the variables explored. Nanoparticle load, acid concentration, temperature, and duration of exposure were deemed significant variables (P<0.05). With an optimal nanoparticle dosage of 550ppm, acid concentration of 0.9 M, temperature of 37°C and exposure time of 3.2 hours imparted an inhibition efficiency of 92.5% and minimized corrosion rate to 0.652 (mm/Y) was achieved on an independent run (validation run), proving that this green synthesized MnO-NPs are a promising agent as an anti-corrosive agent for mild steel.

Data availability

Data created throughout this work are accessible from the corresponding author on request.

Declarations

Conflict of interest

The author declares no competing interests.

Ethical Approval statement

No human and/ or animal studies were involved in this work.

Funding Declaration

No fundswere procured for this work

References

Akinbulumo O.A., Odejobi O.J. and Odekanle E.L. (2020). Thermodynamics and adsorption study of the corrosion inhibition of mild steel by Euphorbia heterophylla L. extract in 1.5 M HCl. *Results in Materials*, **5**, 100074. https://doi.org/10.1016/j.rinma.2020.100074

Al-Amiery A.A., Mohamad A.B., Kadhum A.A.H., Shaker L.M., Isahak W.N.R.W. and Takriff M.S. (2022). Experimental and theoretical study on the corrosion inhibition of mild steel by nonanedioic acid derivative in hydrochloric acid solution. *Scientific Reports*, **12**(1), 4705. https://doi.org/10.1038/s41598-022-08146-8

Amodu O.S., Odunlami M.O., Akintola J.T., Ojumu T.V. and Ayanda O.S. (2022). Artificial neural network and response surface methodology for optimization of corrosion inhibition of mild steel in 1 M HCl by Musa paradisiaca peel extract. *Heliyon*, **8**(12), e11955. https://doi.org/10.1016/j.heliyon.2022.e11955

Aravind J., Kanmani P., Sudha G. and Balan R. (2016). Optimization of chromium (VI) biosorption using gooseberry seeds by response surface methodology. *Global Journal of Environmental Science and Management*, **2**(1), 61–68.

Basik M., Mobin M. and Shoeb M. (2020). Cysteine-silver–gold nanocomposite as potential stable green corrosion inhibitor for mild steel under acidic condition. *Scientific Reports*, **10**(1), 279. https://doi.org/10.1038/s41598-019-57181-5

Birat J.P. (2020). Society, materials, and the environment: The case of steel. *Metals*, **10**(3), 331. https://doi.org/10.3390/met10030331

Boudalia M., Fernández-Domene R.M., Guo L., Echihi S., Belghiti M.E., Zarrouk A., Bellaouchou A., Guenbour A. and García-Antón J. (2023). Experimental and theoretical tests on the corrosion protection of mild steel in hydrochloric acid

environment by the use of pyrazole derivative. *Materials*, **16**(2), 678. https://doi.org/10.3390/ma16020678

Can M. (2020). Green gold nanoparticles from plant-derived materials: An overview of the reaction synthesis types, conditions, and applications. *Reviews in Chemical Engineering*, **36**(7), 859–877. https://doi.org/10.1515/revce-2018-0051

Chandel S.S., Singh P.K., Katiyar P.K. and Randhawa N.S. (2023). A review on environmental concerns and technological innovations for the valorization of steel industry slag. *Mining, Metallurgy and Exploration*, **40**(6), 2059–2086. https://doi.org/10.1007/s42461-023-00886-z

Chitra G., Balasubramani G., Ramkumar R., Sowmiya R. and Perumal P. (2015). Mukiamaderaspatana (Cucurbitaceae) extract-mediated synthesis of silver nanoparticles to control Culex quinquefasciatus and Aedes aegypti (Diptera: Culicidae). *Parasitology Research*, **114**(4), 1407–1415. https://doi.org/10.1007/s00436-015-4320-7

Dash A.R., Lakhani A.J., Devi Priya D., Surendra T.V., Khan M.M.R., Samuel E.J.J. and Roopan S.M. (2023). Green synthesis of stannic oxide nanoparticles for ciprofloxacin degradation: Optimization and modelling using a response surface methodology (RSM) based on the box–Behnken design. *Journal of Cluster Science*, **34**(1), 121–133. https://doi.org/10.1007/s10876-021-02198-y

Devi G.K. and Sathishkumar K. (2017). Synthesis of gold and silver nanoparticles using Mukiamaderaspatna plant extract and its anticancer activity. *IET Nanobiotechnology*, **11**(2), 143–151. https://doi.org/10.1049/iet-nbt.2015.0054

Edoziuno F.O., Adediran A.A., Odoni B.U., Akinwekomi A.D., Adesina O.S. and Oki M. (2020). Optimization and development of predictive models for the corrosion inhibition of mild steel in sulphuric acid by methyl-5-benzoyl-2-benzimidazole carbamate (mebendazole). *Cogent Engineering*, **7**(1), 1714100. https://doi.org/10.1080/23311916.2020.1714100

Eliaz N. (2019). Corrosion of metallic biomaterials: A review. *Materials*, **12**(3), 407. https://doi.org/10.3390/ma12030407

Fadl A.M., Abdou M.I., Hamza M.A. and Sadeek S.A. (2020). Corrosion-inhibiting, self-healing, mechanical-resistant, chemically and UV stable PDMAS/TiO2 epoxy hybrid nanocomposite coating for steel petroleum tanker trucks. *Progress in Organic Coatings*, **146**, 105715. https://doi.org/10.1016/j.porgcoat.2020.105715

Farhadian A., Rahimi A., Safaei N., Shaabani A., Abdouss M. and Alavi A. (2020). A theoretical and experimental study of castor oil-based inhibitor for corrosion inhibition of mild steel in acidic medium at elevated temperatures. *Corrosion Science*, **175**, 108871. https://doi.org/10.1016/j.corsci.2020.108871

González E., Stuhr R., Vega J.M., García-Lecina E., Grande H.J., Leiza J.R. and Paulis M. (2021). Assessing the effect of CeO2 nanoparticles as corrosion inhibitor in hybrid biobased waterborne acrylic direct to metal coating binders. *Polymers*, **13**(6), 848. https://doi.org/10.3390/polym13060848

Gunavathy N. and Murugavel S.C. (2012). Corrosion inhibition studies of mild steel in acid medium using Musa acuminata fruit peel extract. *E-J chem. E-Journal of Chemistry*, **9**(1), 487–495. https://doi.org/10.1155/2012/952402

Heidarzadeh A., Mironov S., Kaibyshev R., Çam G., Simar A., Gerlich A., Khodabakhshi F., Mostafaei A., Field D.P., Robson J.D., Deschamps A. and Withers P.J. (2021). Friction stir welding/processing of metals and alloys: A comprehensive review on microstructural evolution. *Progress in Materials Science*, **117**, 100752. https://doi.org/10.1016/j.pmatsci.2020.100752

Kalaiyarasi M., Nivedha M., Mani M., Harikrishnan R., Kumar J.K., Loganathan S. and Kaviyarasu K. (2024). Synthesis of CuO/NaCuSO4 nanocomposite using an aqueous extract of Tribulus terrestris and their structural, optical, morphology and dielectric studies. *Chemical Papers*, 1–16. https://doi.org/10.1007/s11696-023-03294-1

Kamaraj M., Kamali P., Kaviya R., Abishek K., Navinkumar B., Nithya T., Wong L. and Aravind J. (2024). Human hair biochar to remove malachite green dye and bisphenol-A contamination. *Global Journal of Environmental Science and Management*, **10**(3), 1–12.

Kartsonakis I.A. and Charitidis C.A. (2020). Corrosion protection evaluation of mild steel: The role of hybrid materials loaded with inhibitors. *Applied Sciences*, **10**(18), 6594. https://doi.org/10.3390/app10186594

Kim J., Sovacool B.K., Bazilian M., Griffiths S., Lee J., Yang M. and Lee J. (2022). Decarbonizing the iron and steel industry: A systematic review of sociotechnical systems, technological innovations, and policy options. *Energy Research and Social Science*, **89**, 102565. https://doi.org/10.1016/j.erss.2022.102565

Klinbumrung A., Panya R., Pung-Ngama A., Nasomjai P., Saowalakmeka J. and Sirirak R. (2022). Green synthesis of ZnO nanoparticles by pineapple peel extract from various alkali sources. *Journal of Asian Ceramic Societies*, **10**(4), 755–765. https://doi.org/10.1080/21870764.2022.2127504

Lai C., Xie B., Zou L., Zheng X., Ma X. and Zhu S. (2017). Adsorption and corrosion inhibition of mild steel in hydrochloric acid solution by S-allyl-O, O'-dialkyldithiophosphates. *Results in Physics*, **7**, 3434–3443. https://doi.org/10.1016/j.rinp.2017.09.012

Mohamed Y.M.A., Elgohary E.A. and El Nazer H.A. (2023). Box–Behnken design in optimizing heavy metal removal from wastewater using selenium hybridized graphitic carbon nitride nanocomposites. *Chemical Papers*, 1–8. https://doi.org/10.1007/s11696-023-03226-z

Pitchaipillai, Muthukrishnan & Jeyaprabha, B. & Periakaruppan, Prakash. (2013). Adsorption and corrosion inhibiting behavior of Lannea coromandelica leaf extract on mild steel corrosion. *Arabian Journal of Chemistry*. **7**. https://doi.org/10.1016/j.arabjc.2013.08.011.

Raabe D. (2023). The materials science behind sustainable metals and alloys. *Chemical Reviews*, **123**(5), 2436–2608. https://doi.org/10.1021/acs.chemrev.2c00799

Sandhu Z.A., Raza M.A., Farwa U., Nasr S., Yahia I.S., Fatima S., Munawar M., Hadayet Y., Ashraf S. and Ashraf H. (2023). Response surface methodology: A powerful tool for optimizing the synthesis of metal sulfide nanoparticles for dye degradation. *Materials Advances*, **4**(21), 5094–5125. https://doi.org/10.1039/D3MA00390F

Singh N.K., Cadoni E., Singha M.K. and Gupta N.K. (2013). Dynamic tensile and compressive behaviors of mild steel at wide range of strain rates. *Journal of Engineering Mechanics*, **139**(9), 1197–1206. https://doi.org/10.1061/(ASCE)EM.1943-7889.0000557

Souri M., Hoseinpour V., Shakeri A. and Ghaemi N. (2018). Optimisation of green synthesis of MnO nanoparticles via

utilising response surface methodology. *IET Nanobiotechnology*, **12**(6), 822–827. https://doi.org/10.1049/iet-nbt.2017.0145

Tamilselvi B., Bhuvaneshwari D.S., Karuppasamy P., Padmavathy S., Nikhil S., Siddegowda S.B. and Ananda Murthy H.C. (2024). Investigation of corrosion inhibition of mild steel in 0.5 M H2SO4 with Lachanceafermentati inhibitor extracted from rotten grapefruits (Vitis vinifera): Adsorption, thermodynamic, electrochemical, and quantum chemical studies. *ACS Physical Chemistry Au*, **4**(1), 67–84. https://doi.org/10.1021/acsphyschemau.3c00055

Yang W., Feng W., Liao Z., Yang Y., Miao G., Yu B. and Pei X. (2021). Protection of mild steel with molecular engineered epoxy nanocomposite coatings containing corrosion inhibitor functionalized nanoparticles. *Surface and Coatings Technology*, **406**, 126639. https://doi.org/10.1016/j.surfcoat.2020.126639

Ying S., Guan Z., Ofoegbu P.C., Clubb P., Rico C., He F. and Hong J. (2022). Green synthesis of nanoparticles: Current developments and limitations. *Environmental Technology and Innovation*, **26**, 102336. https://doi.org/10.1016/j.eti.2022.102336